5 years of *in situ* reinforcement corrosion monitoring in the splash and submerged zone of a cracked concrete element

A. Michel[a,c] , H.E. Sørensen[b], M.R. Geiker[c]

[a)] *Technical University of Denmark (DTU), Department of Civil Engineering, Kgs. Lyngby, Denmark*

+45 4525 1656, +45 4588 3282, almic@byg.dtu.dk, http://www.dtu.dk

[b)] *Danish Technological Institute (DTI), Building and Construction, Taastrup, Denmark*

[c)] *Norwegian University of Science and Technology (NTNU), Department of Structural Engineering, Trondheim, Norway*

Abstract

Results of more than 5 years of *in situ* reinforcement corrosion monitoring are presented including continuous measurements of concrete resistivity, temperature, and open circuit corrosion potential measurements. Depth dependent resistivity and temperature measurements were obtained by means of multi-ring electrodes, while so-called instrumented rebars were used for location- and time-dependent open circuit corrosion potential measurements. The presented results highlight the complex interaction between mass transport, fracture, exposure, and electrochemistry and underline the importance of *in situ* measurements, which are imperative for model testing to enable accurate and reliable long-term performance predictions of reinforced concrete structures.

Keywords: Corrosion, Cracked concrete, Monitoring, Concrete resistivity, Open circuit corrosion potential

1 Introduction

The durability, and in particular corrosion, of reinforced concrete structures remains a considerable societal challenge despite many years of practical experience and a large number of extensive research programs. Although many questions remain unanswered [1], the development of more advanced modelling tools has contributed to an increased understanding of the underlying mechanisms and processes related to corrosion in reinforced concrete structures. Noteworthy in this context is the development of multi-physics and multi-scale modelling approaches combining *e.g.* mass transport, electrochemistry, and fracture mechanics, see *e.g.* [2–6]. While these models help to shed light on some of the governing mechanism for concrete durability, these tools require a large number of input parameters as well as extensive experimental data for model testing and validation. However, the majority of available data on reinforcement corrosion is based on short-term laboratory experiments, see *e.g.* [7–10]. While results of such laboratory studies are often only suitable for limited validation and testing of advanced modelling tools, such as mass transport of selected species [11–13], mechanical properties [14,15], *etc*., other important parameters affecting the durability of reinforced concrete as well as relations between governing mechanisms are often not captured. Realistic environmental boundary conditions, simultaneous deterioration mechanisms, *etc*. can only be studied on *in situ* specimens. However, this requires, apart from a long-term commitment, specimens with a large number of sensors to capture all relevant parameters and material properties needed for validation and calibration of advanced modelling tools. While there are a number of exposure sites, experimental investigations and studies have mainly focused on chloride ingress as the governing mechanism in connection to reinforcement corrosion, see *e.g.* [16–18]. Other parameters, such as temperature, electrolyte resistivity, open circuit corrosion potential, *etc.*, known to have a considerable influence on concrete deterioration and reinforcement corrosion in particular [19,20] are scarcely reported in the literature. Thus, in order to test, calibrate, and validate recently developed advanced modelling tools for reinforced concrete deterioration, experimental data from *in situ* specimens are needed.

This investigation reports the results of more than 5 years of *in situ* reinforcement corrosion monitoring. To study deterioration processes (in particular reinforcement corrosion) in reinforced concrete, one test specimen was prepared and instrumented for continuous monitoring. The measurement campaign included thereby monitoring of concrete resistivity, temperature, and open circuit corrosion potential measurements. Depth dependent resistivity and temperature measurements were obtained by means of multi-ring electrodes, while so-called instrumented rebars [21] were used for location- and time-dependent open circuit corrosion potential measurements. Before exposure of the specimen in the immersed- and the splash zone of Rødbyhavn, Denmark, two bending cracks were introduced to facilitate initiation and propagation of reinforcement corrosion. Discussion of the results focuses on the relation between temperature and resistivity as well as various impacts on the open circuit potential in the context of reinforcement corrosion. Among others, cycles of OCP were observed, *i.e.* indicating depas-

sivation and repassivation, with a duration of several years. This discontinuous state of corrosion underlines the importance of continuous monitoring to understand the mechanisms of corrosion initiation and propagation and ultimately the service life of structures.

2 Experimental

2.1 Materials and specimen preparation

For the experimental investigations, one instrumented reinforced concrete element was cast, see Figure 1. Plain Portland cement (see Table 1) and a water-to-cement ratio of 0.40 were used; the mix design of the concrete is given in Table 2. As reinforcement five conventional rebars with 12 mm diameter and two instrumented rebars with 25 mm diameter (described in Section 2.3.3) were embedded vertically with a cover depth of 87.5 mm in the 1,000 × 2,000 × 200 mm^3 (length × height × width) concrete element (see Figure 1; stirrups are not shown). The concrete was mixed using a concrete mixing plant with a 250 l capacity. Aggregates were first mixed dry for 30 seconds. Afterwards, cement was added and mixing continued for another 30 seconds. Subsequently, water was added over a period of 30 seconds while mixing, followed by the addition of an air entraining agent and (with a 30 second delay) superplasticizer. Mixing continued for 120 seconds after the addition of superplasticizer, *i.e.* a total of 240 seconds. For the production of the concrete block, two batches of concrete were required. Homogenization of the concrete batches was performed in a 500 l pan mixer. The concrete was subsequently discharged into a crane bucket, which was used for filling of the formwork. The concrete was cast from the top of the formwork (and the final element) with a maximum drop height of approximately 2.2 m. The concrete was cast in five subsequent layers and each layer was compacted individually by a small poker vibrator. After casting, the form was stored at laboratory conditions (*i.e.* 18 ± 2 °C) covered with plastic for 48 hours. Upon demoulding, the concrete element was cured sealed in plastic at laboratory conditions for additional 68 days. Subsequently, the specimen was cracked horizontally at two locations by means of three point bending: approximately 0.7 m and 1.7 m from the top (crack 1 and crack 2, respectively see Figure 1). Three pairs of measuring points were glued along the anticipated crack path and the crack width was measured during and after the cracking with a DEMEC Mechanical Strain Gauge. Upon cracking, two recesses were cut at the edges of the concrete block and filled with fast hardening repair mortar to retain induced crack widths (see Table 3). The repair mortar was allowed to cure sealed for 24 hours before unloading. After cracking, the specimen was stored seven months on-site, still sealed in plastic until exposure.

Table 1: Oxide composition of cement, after [22].

	CaO	SiO_2	Al_2O_3	Fe_2O_3	SO_3	MgO	TiO_2	P_2O_5	CO_2	LOI	Na_2O
Mass %	65.6	24.8	2.9	2.3	2.2	0.8	0.1	0.2	0.2	0.7	0.7

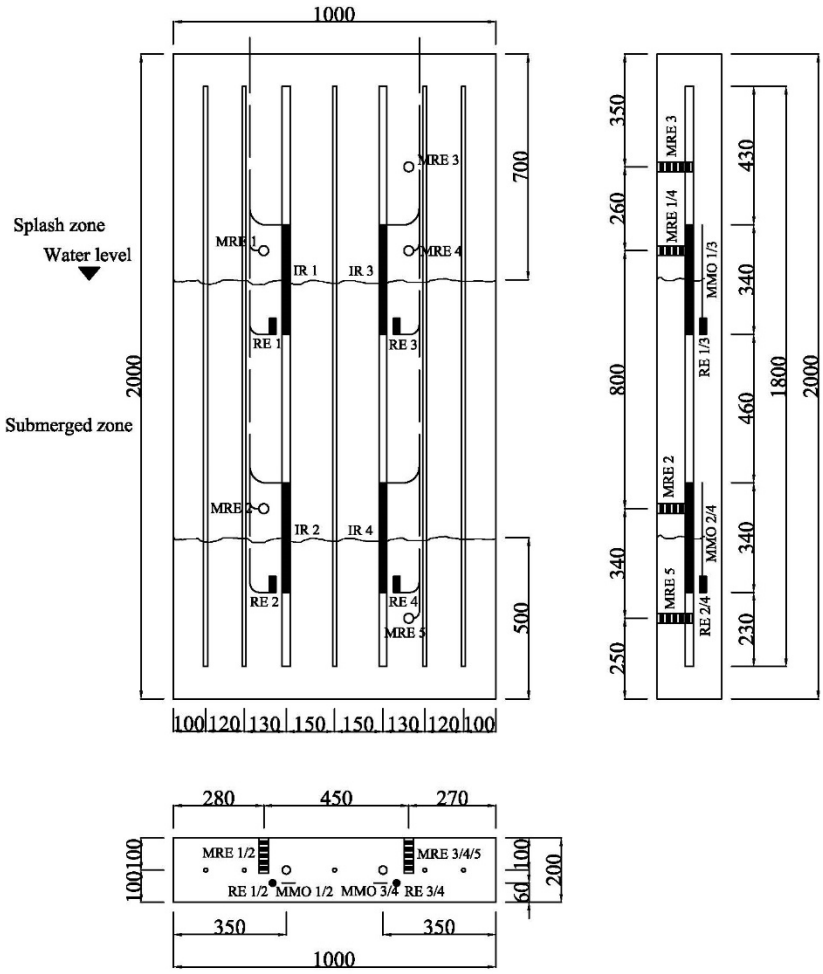

Figure 1: Element geometry along with type and location of sensors, *i.e.* multi-ring electrodes (MRE), reference electrodes (RE), and instrumented rebars (IR). Position of mean water level is shown; see Section 0 for variations. All dimensions in [mm].

2.2 Exposure

The specimen was exposed to sea water at an exposure site in the Rødbyhavn area in Denmark. The chloride content of the sea water is approximately 0.7% [23] and annual temperature variations of the sea water range typically from -1 to 20°C. The specimen was partly immersed in the seawater, with the upper 0.7 m above the mean water level, see Figure 1. While the regular tide is only 0.1 m, normal water level variations are ±1.1 m and extreme variations are ±2.0 m [23], see Figure 2.

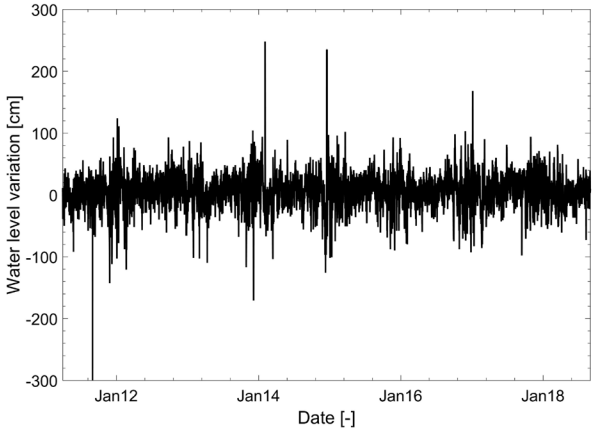

Figure 2: Water level variation during monitoring period.

Table 2: Composition of investigated concrete element.

Constituent	[kg/m^3]
Cement	368.5
Water	143.3
Sand (0-2 mm)	699.6
Gravel (4-8 mm)	379.8
Stones (8-16 mm)	267.5
Stones (16-22 mm)	532.2
Air entraining agent	1.7
Superplasticizer	3.0
Total	2395.7
Free water	147.0
w/c-ratio	0.4
Air content	3.8%

Table 3: Crack width in [mm] before and during exposure of specimen.

	Crack 1			Crack 2		
	Point 1	Point 2	Point 3	Point 1	Point 2	Point 3
Apr 2011	0.23	0.18	0.24	0.23	0.18	0.24
Apr 2012	0.26	0.22	0.31	0.26	0.22	0.31

2.3 Sensors and data acquisition

The concrete element was instrumented with a number of sensors to monitor open circuit potential (OCP), resistivity, and temperature. So-called instrumented rebars and reference electrodes were used for time- and location dependent open circuit potential measurements, while multi-ring electrodes were used for depth- and time dependent temperature and resistivity measurements. An overview of the

specimen geometry along with type and location of all sensors is provided in Figure 1. More detailed information on the individual sensors as well as the data acquisition is given in the following sections.

2.3.1 Multi-ring electrodes (MRE)

Combined temperature and resistivity measurement were undertaken by means of multi-ring electrodes (MRE). The MRE consists thereby of several stainless steel rings, which are kept at distance from each other by isolating plastic rings. Typically, the electrode is produced with nine stainless steel rings providing eight measurement points and a pt1000 temperature sensor. The total length of the MRE is thereby 50 mm with a diameter of 20 mm and a ring spacing of 5 mm, thus, providing 5 mm increments for depth measurements). Electrical connection of the rings is realized by cables that are running inside the electrode without disturbing the surrounding concrete. The remaining inside of the electrode is filled with epoxy. Between each pair of neighboring steel rings, the electrolyte resistance can be measured and a local resistance profile of the concrete can be created. Determination of the resistance is realized by impedance measurements at a measuring frequency of 108 Hz to avoid polarization effects at the electrodes. The measured resistance values can be converted to specific resistivity values through a sensor specific transfer factor, the so-called cell constant, which can be derived from experimental tests in aqueous solution of known resistivity [24]. The measured resistivity provides furthermore the possibility to determine indirectly the moisture content of the concrete, since the resistivity is among others (highly) moisture dependent, see *e.g.* [19,25,26]. For a quantitative determination of the moisture content, the dependence of the resistivity on temperature, ion concentration, and concrete composition (in particular the cement type) has to be taken into account [27]. To account for these dependencies, calibration curves can be used relating the resistivity to the moisture content.

2.3.2 Reference electrodes (RE)

For open circuit potential measurements of the individual pins of the instrumented rebar sections (see Section 2.3.3), ERE 20 reference electrodes were used [28]. Four reference electrodes were placed in the vicinity of the instrumented sections of the 25 mm rebars, see Figure 1. The reference electrodes use a manganese dioxide electrode in steel housing with an alkaline, chloride-free gel and a porous cement plug at one end. The steel housing is made of a corrosion resistant material and the pH of the gel corresponds to that of pore water in normal concrete, reducing errors due to low diffusion of ions through the porous cement plug. The potential of each reference electrode was measured against a saturated calomel electrode and provided by the producer.

2.3.3 Instrumented rebars (IR)

Two rebars with 25 mm diameter were embedded in the concrete block to allow for macrocell current as well as time- and location dependent open circuit corrosion potential (OCP) measurements. Each of the rebars contained two instrumented sections to enable the intended electrochemical measurements. An illustration of the design of the instrumented rebar section is given in Figure 3. The ability of the instrumented rebar sections to enable macrocell current as well as time- and location dependent OCP measurements in concrete, while having a comparable mechanical behavior as a conventional rebar,

was presented in *e.g.* [6,21,29]. Each section of the instrumented rebar was thereby made from three parts of standard 25 mm diameter deformed rebar cut to size and connected by means of screw threads. To provide a 6 mm diameter void along the center of the instrumented rebar, the midsection was hollowed. Hollowing of the instrumented rebar led to a reduction in bending stiffness (*i.e.* 0.3 %) and cross sectional area (*i.e.* 6 %) as well as an axial stiffness corresponding to a standard rebar with a 24.74 mm nominal diameter [29]. Subsequently, seventeen holes (with a 3.5 mm diameter and a 15 mm spacing) were bored through the surface of the instrumented rebar section. Thereafter, a 3 mm steel pin was placed in each hole and a lead wire was soldered to each of the steel pins [29]. To ensure electrical disconnection between the rebar and individual steel pins, each of the pins was enclosed in glue-coated heat-shrink tube. Finally, to protect the rebar, individual steel pins, and wires, the hollowed mid-section was filled with epoxy resin. The two solid rebar sections were connected to the hollowed mid-section using threaded connections. [29]

Open circuit corrosion potentials of all sensors along instrumented rebars IR 3 and IR 4 were measured against ERE 20 reference electrodes (see Section 2.3.2), which were placed in the vicinity of instrumented sections of the rebar. For macrocell current measurements, an electrical connection between the counter electrode and working electrode (individual sensors along instrumented rebars IR 1 and IR 2) were established over a zero-impedance-ammeter without introducing resistance to the system [29]. As counter electrode, a ruthenium/iridium mixed metal oxide activated titanium mesh (MMO) was used, which was placed in the vicinity of the instrumented rebar. Once the individual steel pins were connected to the MMO, a macrocell current flow through the ammeters was allowed (without introducing resistance) and the mixed corrosion potential was attained [29]. Nevertheless, it should be noted that only the macrocell current between the dissimilar metals is measured in such a configuration and accordingly the micro- and macrocell corrosion activity on the preferential corroding metal surface is not reflected [29]. However, due to its simplicity and clear indication of corrosion initiation by a sharp rise in macrocell current upon depassivation, the technique is frequently used in the area of reinforcement corrosion [29], see *e.g.* [30,31].

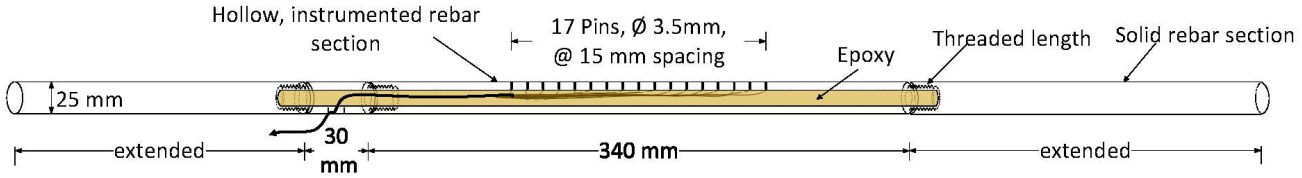

Figure 3: Design of instrumented rebar section for time- and location dependent OCP and macrocell current measurements (Note: ribs are not shown in sketch), after [21].

2.3.4 Data acquisition

The data logging system consisted of a personal computer (PC), a number of customized switchboards, 3G cellular modem, nine-channel amplifier, and optical interface. Data from the instrumented rebars

and multi-ring electrodes was stored on the PC, which was located at the exposure site. The 3G cellular modem allowed for remote access to the PC and file transfer of logged data. Customized switchboards were used for measurements of open circuit potentials and macrocell current for the instrumented rebars (see Section 2.3.3). Up to 16 channels, *i.e.* one channel per pin and per instrumented rebar section, were recorded with each switchboard and measurements were undertaken continuously against the reference electrodes (see Section 2.3.2) and ruthenium/iridium mixed metal oxide activated titanium mesh, respectively. However, data was only stored if at least one out of the 16 measurements per instrumented rebar section differed more than 10 mV (for open circuit potential) or 5 µA (for macrocell current) from the last stored value. The individual multi-ring electrodes (see Section 2.3.1) were connected to a nine-channel amplifier and subsequently via an optical interface and standard USB cable connected to the PC. Measurements of temperature and resistivity with the multi-ring electrodes were undertaken on an hourly basis.

3 Results

Results of more than 6.5 years of *in situ* monitoring (June 2011 - January 2018) of a cracked concrete element exposed to varying environments in the harbor of Rødbyhavn, Denmark, are presented in the following. Results include crack distance- and time dependent open circuit corrosion potential measurements by means of instrumented rebars and surface depth- and time dependent temperature and resistivity measurements at various locations of the concrete element, see Table 4 and Figure 1. Instrumented rebars IR 1 and IR 2, designed for macrocell current measurements, failed to record any data during the exposure period and are not discussed in the following. MREs stopped recording data after approximately five years.

Table 4: Overview of sensors, type of recorded data, and sensor location.

Sensor name	Data	Location	Comments
MRE 1	Resistivity and temperature	Splash zone	Failed after 6 months
MRE 2		Submerged zone	Stopped after 5 years
MRE 3		Top of splash zone	Stopped after 5 years
MRE 4		Splash zone	Stopped after 5 years
MRE 5		Submerged zone	Stopped after 5 years
IR 1 / MMO 1	Corrosion current	Splash zone	Failed
IR 2 / MMO 1		Submerged zone	Failed
IR 3 / RE 3	Open circuit potential	Splash zone	Still operating
IR 4 / RE 4		Submerged zone	Still operating

3.1 Data processing

Data was either recorded at a fixed interval, *i.e.* one hour in case of resistivity and temperature measurements by means of multi-ring electrodes (MRE), or due to a relative change in open circuit potential

for location-dependent measurements for instrumented rebars. Within the MRE data, single measurements in form of a sudden increase in resistivity of around 200 – 400 Ωm were recorded randomly, see Figure 4. To eliminate these outliers and reduce noise in the recorded data, the raw data was initially processed. The procedure included filtering of outliers, erroneous data, and smoothing applying a 1-dimensional median filter. In addition, a moving average filter was applied for better illustration of correlations between recorded data. The data processing procedure is illustrated by means of an example for one depth measurement of MRE 1 in Figure 4.

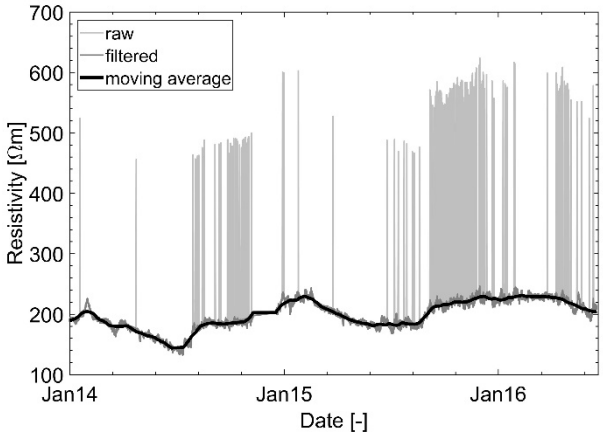

Figure 4: Example of data processing procedure for resistivity measurements from MRE 2 at a depth of 6.25 mm (for location of sensor, see also Figure 1).

3.2 Resistivity and temperature

Results (after data processing, see Section 3.1) of depth- and time dependent resistivity and temperature measurements for various locations in the cracked concrete element are illustrated in Figure 5 and Figure 6, respectively. In general, the results indicate no significant difference in concrete resistivity for sensors located in the lower part of the splash zone and submerged zone, *i.e.* MRE 1, 2, 4, and 5. Concrete resistivity is varying between approximately 150 and 500 Ωm, whereas the maximum values are found in the outer 30 to 40 mm region of the specimen. For deeper depths, *i.e.* 40 to approximately 100 mm, similar values for the concrete resistivity (between 150 and 250 Ωm) are observed independent of the sensor location in the specimen. Considerable higher values for the concrete resistivity, *i.e.* up to approximately 4000 Ωm, are only observed for sensor MRE 3 located at the top of the splash zone. However, these high values were only measured for the outer 30 to 40 mm region of the specimen, for depths above 40 mm similar resistivity values were observed as for the other MREs.

Results for temperature measurements are illustrated in Figure 6. From the presented results, it can be seen that temperature profiles are comparable for all sensors locations in the concrete block, *i.e.* splash as well as submerged zone. Lowest temperature values are found during the winter with around 0 °C while highest temperatures are observed in the summer with around 20 to 25 °C. No significant temperature gradient over the depth of the cracked concrete element is observed from the presented results.

Seasonal variations are observed for both resistivity and temperature, variations in the measured concrete resistivity follow thereby seasonal trends in observed temperature; *i.e.* an increase in temperature is associated with a decrease in resistivity, while a decrease in temperature leads to an increase in resistivity.

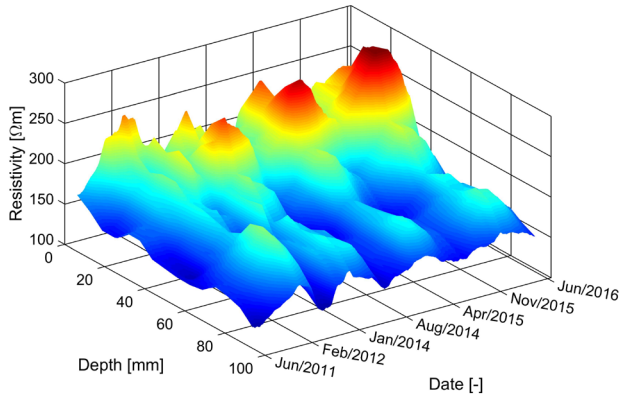

a) MRE 1

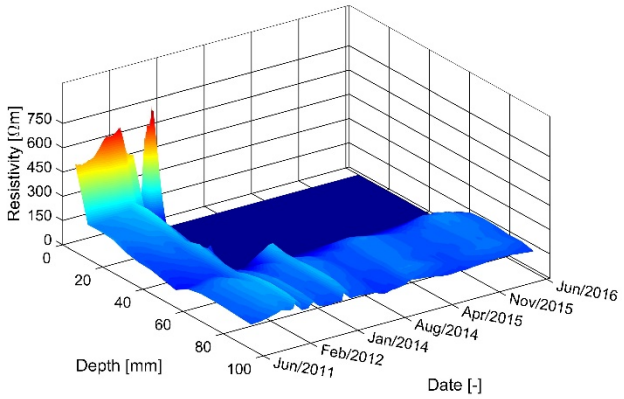

b) MRE 2

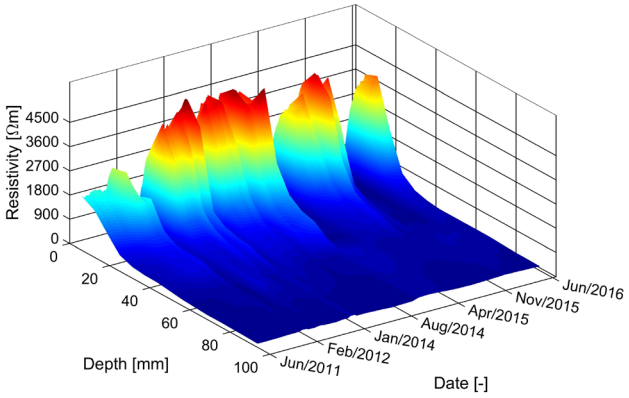

c) MRE 3

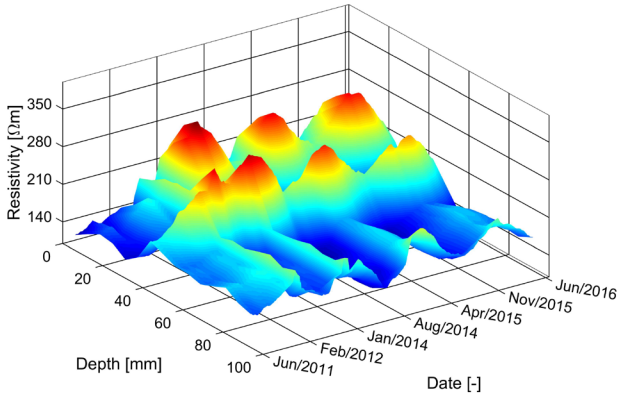

d) MRE 4

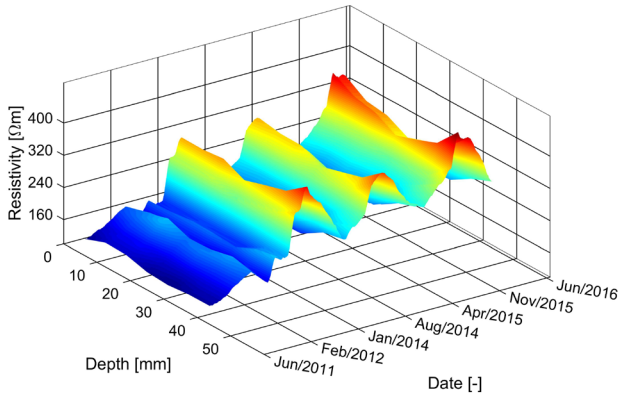

e) MRE 5

Figure 5: Concrete resistivity measurements along the specimen depth over a period of 5 years and for various locations, a) MRE 1, b) MRE 2, c) MRE 3, d) MRE 4, and e) MRE 5, (for location of sensor, see also Figure 1). Please note: part of sensor MRE 1 failed after approximately six months of exposure and no resistivity data was measured after that period.

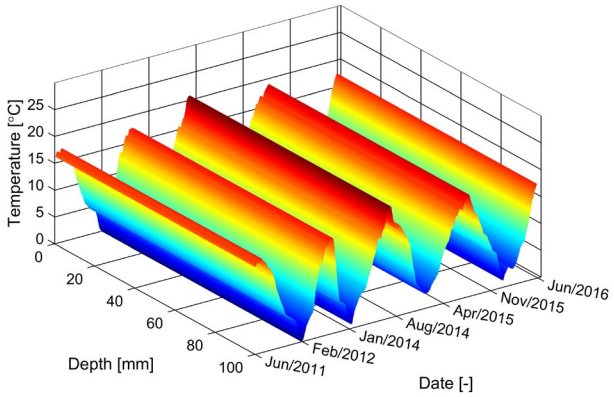

a) MRE 1

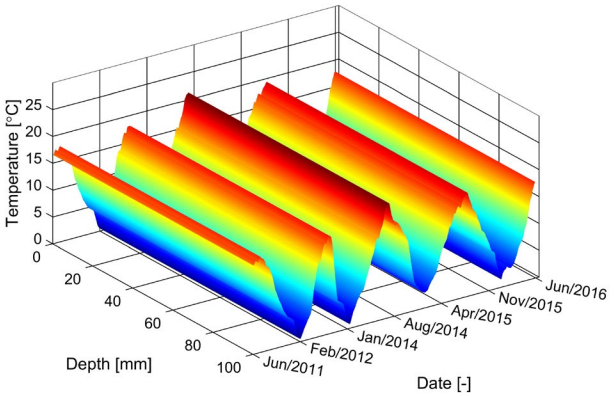

b) MRE 2

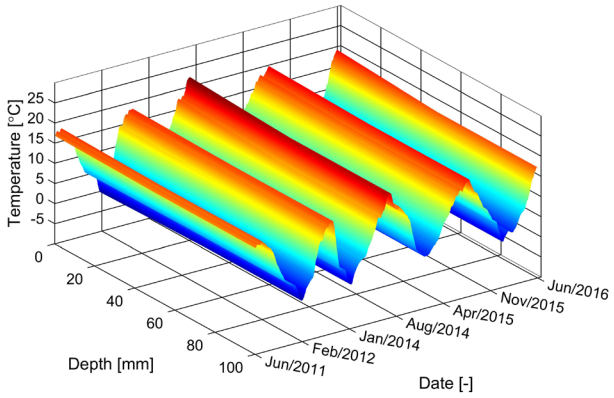

c) MRE 3

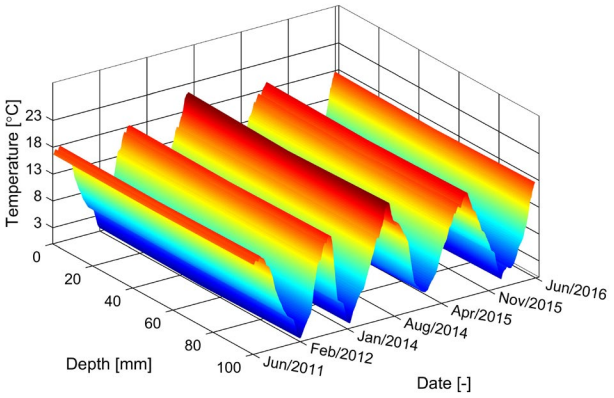

d) MRE 4

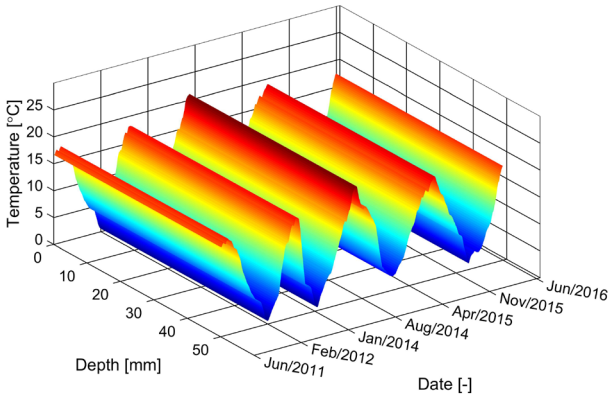

e) MRE 5

Figure 6: Temperature measurements along the specimen depth (*i.e.* at 50 and 100 mm) over a period of 5 years and for various locations, a) MRE 1, b) MRE 2, c) MRE 3, d) MRE 4, and e) MRE 5, (for location of sensor, see also Figure 1).

3.3 Open circuit corrosion potential (OCP)

Contour plots illustrating results of all sensor locations along the instrumented rebars, *i.e.* IR 3 and 4, for the cracked concrete element are shown in Figure 7. Results are presented as a function of the exposure time and location from the crack (in mm) as well as OCP (in mV_{SCE}), which is indicated by a color scale. Results in terms of OCP measurements are thereby presented for a region between -120 mm and 105 mm from the corresponding bending cracks.

Initially, corrosion potentials around -200 to 0 mV_{SCE} were measured for all sensors along instrumented rebar IR 3 and IR 4 (see Figure 7 a and b), respectively. With progressing exposure time, individual sensors located between - 15 mm and -120 mm from the bending crack showed a considerable decrease in OCP for instrumented rebar IR 3 located in the splash zone. Sensors located outside this region (*i.e.* in the region between 0 mm and 105 mm), showed no decrease in OCP throughout the exposure period indicating no change in corrosion state, *i.e.* the sensors remained in the passive state. For the instrumented rebar IR 4 located in the submerged zone, a decrease in OCP was observed for individual sensor in a region between – 120 mm and 105 mm from the corresponding crack. For both instrumented rebars the drop resulted in OCPs around – 1000 mV_{SCE}. The OCP measurements indicate thereby that with increasing distance from the crack, initiation of corrosion was delayed. Furthermore, presented results indicate that active corrosion stops after around 1½ years in October 2014 and OCPs for individual sensors are in range of -200 to 0 mV_{SCE} as measured at the beginning of exposure. However, a decrease in OCP is observed for individual sensors of instrumented rebars IR 3 and IR 4 again in July 2016. This second period of active corrosion appears to last for only 3-4 months after which an increase in OCPs is observed to values similar as at the start of exposure, *i.e.* -200 to 0 mV_{SCE}. Active corrosion is thereby observed within a limited area for IR 3, *i.e.* – 45 to – 60 mm from the crack, while the decrease in OCP for IR 4 is less pronounced. A third active period is observed from July 2018 to October 2018. However, the potential drop is considerable smaller compared to the first and second active phase, *i.e.* around 200 mV_{SCE}. Thereafter, OCPs for individual sensors are in range of -200 to 0 mV_{SCE} as measured at the beginning of exposure.

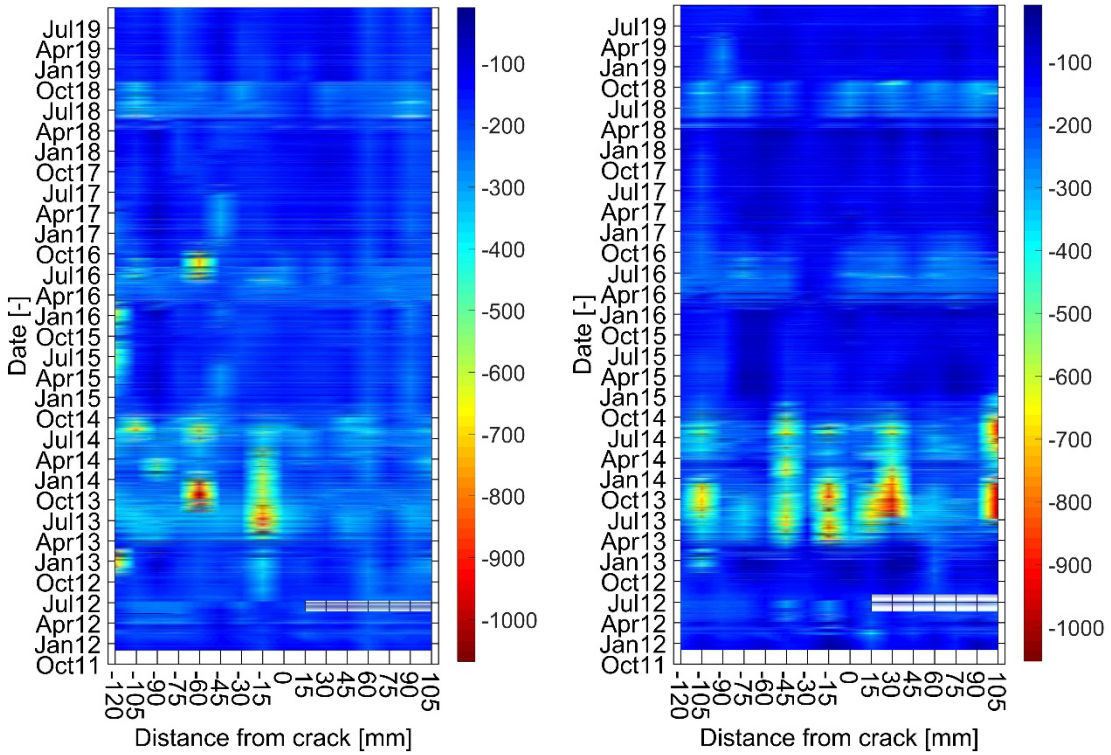

a) IR 3 b) IR 4

Figure 7: Development of open circuit corrosion potential in [mV_{SCE}] over time [month and year] for instrumented rebar 3 (IR 3) in the splash zone and instrumented rebar 4 (IR 4) in the submerged zone (for location of sensor, see also Figure 1).

4 Discussion

Results of more than 5 years of *in situ* monitoring covering open circuit corrosion potential (OCP) measurements by means of instrumented rebars as well as resistivity and temperature using multi ring electrodes are discussed in the following. Motivation for initiating such a campaign was rooted in the fact that experimental data from *in situ* specimens are needed in order to test, calibrate, and validate recently developed advanced modelling tools for reinforced concrete deterioration, see *e.g.* [2–6]. However, it is acknowledged that neither destructive measurements, including *e.g.* chloride profiles, nor visual observations of corrosion and self-healing, crack morphology, concrete-steel interface properties (*e.g.* pores, bleeding zones, *etc.*), *etc.* are available at this point. Such investigations are planned once the current measurement campaign is finished including in-depth analysis for the premature failure of some sensors (see also Table 4).

4.1 Temperature and resistivity profiles

While no significant temperature gradients along the depth of the concrete element were observed, depth dependent resistivity profiles were measured (compare Figure 5 and Figure 6). Depth- and time dependent resistivity measurements indicated thereby similar values (between 150 and 250 Ωm) for

concrete resistivity in the splash and submerged zone, for locations deeper than approximately 40 mm, see Figure 8. A considerable change in resistivity over the concrete depth was only observed for the sensor located in the top of the splash zone; see Figure 8 a) and for a depth of around 30 to 50 mm (in which the reinforcement usually is placed for most structures), which is in the same order of magnitude as *e.g.* reported in [32,33] for a wide range of concretes.

Concrete resistivity is affected by a number of factors such as the pore structure, composition of pore solution, cementitious content, w/c ratio, moisture content, *etc.*, see *e.g.* [34–36]. In addition, temperature is known to have a considerable effect on the concrete resistivity, see *e.g.* [37,38]. For constant moisture conditions, an increase in temperature is associated with a decrease in resistivity and *vice versa*. This behavior is generally observed for the sensors (see Figure 8), except for the outer region of the sensor located in the top of the splash zone (MRE 3). For this region, an increase in resistivity is observed for increasing temperatures. This counter intuitive observation, might be caused by other effects such as advective mass transport (*e.g.* drying and wetting) and possible microstructural changes as well as combinations of these. Due to the repeated behavior (see Figure 8 a), it is expected that advective mass transport in the top of the element is the governing phenomenon overruling the influence of temperature on the concrete resistivity of sensor MRE 3.

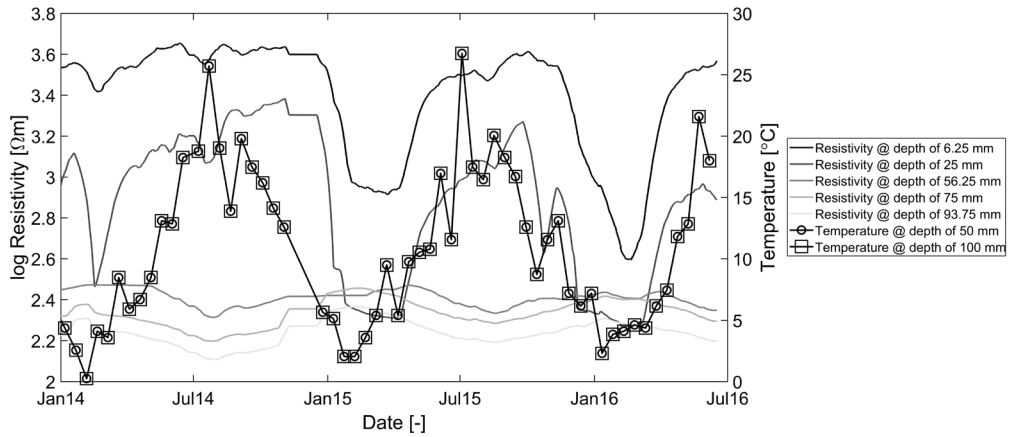

a) MRE 3

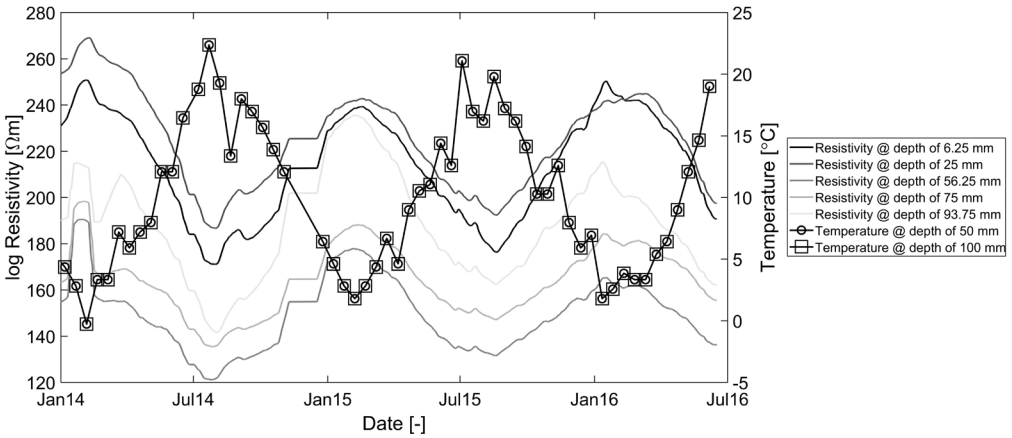

b) MRE 4

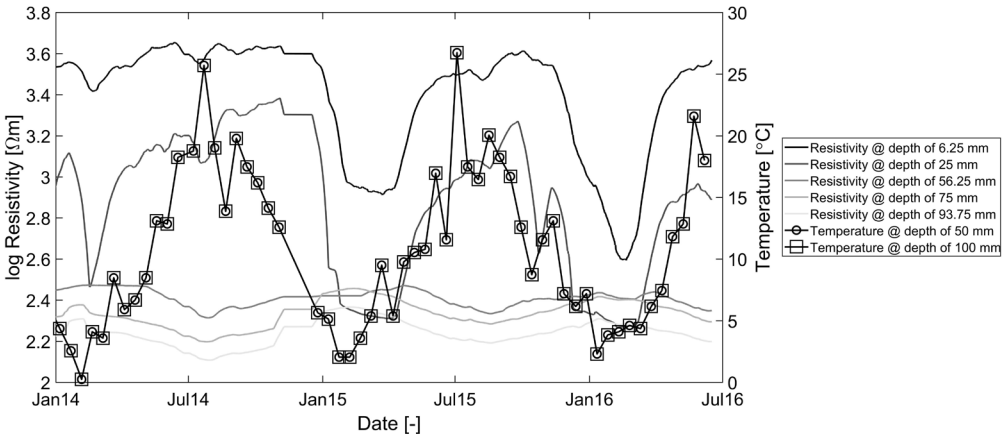

c) MRE 5

Figure 8: Comparison between resistivity and temperature for selected locations and exposure time, a) MRE 3 (top of splash zone), b) MRE 4 (splash zone), and c) MRE 5 (submerged zone), (for location of sensor, see also Figure 1).

4.2 Open circuit corrosion potentials

Comparisons of contour plots presented in Section 3.3 (see Figure 7), show similar open circuit corrosion potentials (OCPs) at the beginning of exposure for the two instrumented rebars located in the splash and submerged zone, respectively. Initially, OCPs of approximately -200 to 0 mV_{SCE} were measured indicating a passive corrosion state of the reinforcement. Similar OCP values for passive reinforcement are reported in the literature in oxygen containing concrete, see *e.g.* [21,39].

With progressing time, an either gradual decrease or sudden drop in OCP was observed for sensors along the instrumented rebar indicating active corrosion was thermodynamically favored. For the instrumented rebar located in the splash zone (IR 3), a sudden decrease in potential was observed for the majority of the sensors (see *e.g.* Figure 10), while for the instrumented rebar located in the submerged zone (IR 4) a gradual drop in OCP was mainly observed. OCPs for IR 3 and 4 decreased to values between approximately -1000 mV_{SCE} and -500 mV_{SCE}, which is in good agreement with values that have been reported in the literature for active corrosion, see *e.g.* [40,41]. OCP values indicating active corrosion were first observed around April 2013 after almost two years of exposure for both sensor locations. This observation is in strong contrast to many laboratory investigations that have reported an expedited corrosion initiation in cracked concrete, see *e.g.* [7,8,29,42–44]. The comparable long time to corrosion initiation may be related to initial self-healing [45], although the time from cracking to exposure and in particular the moisture load during that period were limited. Additional reasons may be linked to the extent of concrete-steel interface damage, *i.e.* slip and separation, which may differ from other studies due to surface crack width and large cover depth in the concrete element [29].

In addition, cyclic behavior of OCP was observed indicating depassivation and repassivation of the pins. Active corrosion continued to a varying extent for a period of approximately one and a half years for both sensor locations. The cyclic behavior of the OCP observed in the cracked element may be owed to self-healing [45] (partly) restoring the concrete-steel interface damaged in the cracking process by slip and separation [46] followed by subsequent chloride ingress and repeated corrosion initiation.

Although, there appears to be a connection between a decrease in resistivity and drop in OCP around July 2014, no general correlation between OCP and resistivity (and thus temperature), neither in the splash nor in the submerged zone was observed. Within the first active corrosion period (between April 2013 and October 2014) and after, the concrete resistivity cycled through several minima and maxima without a significant change in OCP, see Figure 9. However, it should be noted that a recent literature review [47] revealed pronounced effects on the initiation of reinforcement corrosion for the moisture state (and thus resistivity). Hence, further research in corrosion of steel in concrete should focus also on the working mechanisms related to the moisture conditions in microscopic and macroscopic voids at the steel-concrete interface [47].

While similar OCP values indicating initiation of reinforcement corrosion were observed for sensors in the splash and submerged zones, the time to corrosion initiation and duration of corrosion varied for IR 3 and IR 4. To determine the time to corrosion initiation for active sensors of IR 3 and 4 from the experimental data, the procedure outlined in [48] was adopted, in which active corrosion is assumed when the recorded potential is lower than a prescribed threshold. The concept is illustrated in Figure 10 a) for IR 3 located in the splash zone and OCP thresholds indicating 90 % probability (*i.e.* -477 mV_{SCE}) and severe corrosion (*i.e.* -627 mV_{SCE}) according to [48]. For the determination of the time to corrosion initiation of sensor pins the OCP threshold for 90 % corrosion was chosen. The “relative” time to corrosion initiation for the various sensors along the instrumented rebars is then calculated as the time difference between the first recorded corrosion initiation and subsequent locations of corrosion. Results of the analysis are presented in Figure 10 b), showing an increase in time to corrosion initiation with increasing distance from the crack for active pins (please note exception for sensor located at -120 mm from crack). The highly nonlinear increase in time to corrosion initiation indicates that the process may be controlled by a combination of transport mechanisms (advection, diffusion) along the instrumented rebars.

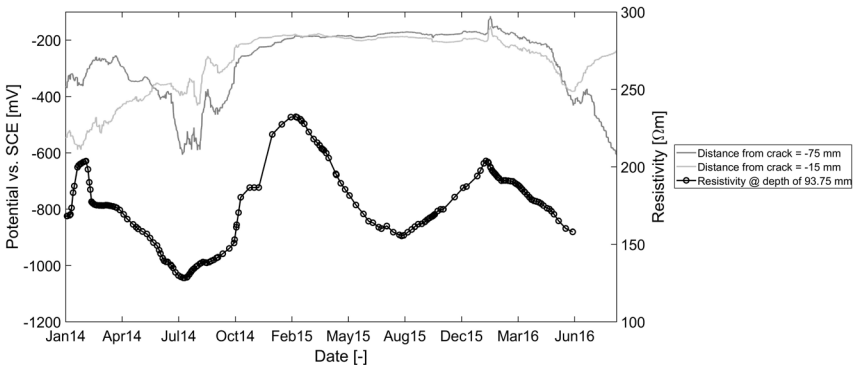

a) IR 3 and MRE 3

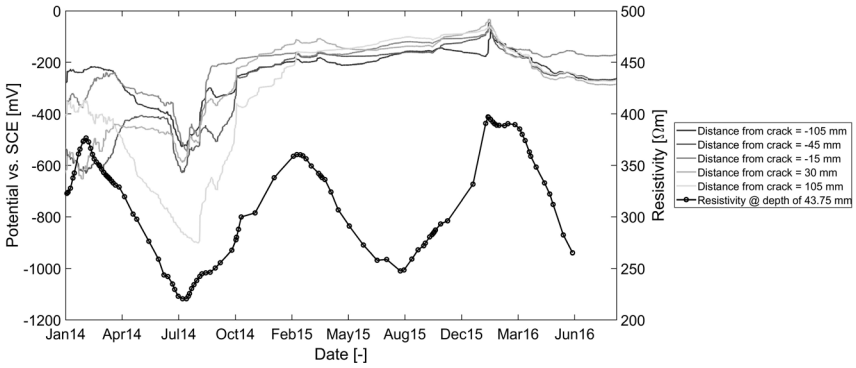

b) IR 4 and MRE 5

Figure 9: Comparison of open circuit corrosion potential (OCP) and concrete resistivity for selected locations and exposure time: a) IR 3 and MRE 3 in the splash zone and b) IR 4 and MRE 5 in the submerged zone (for location of sensor, see also Figure 1).

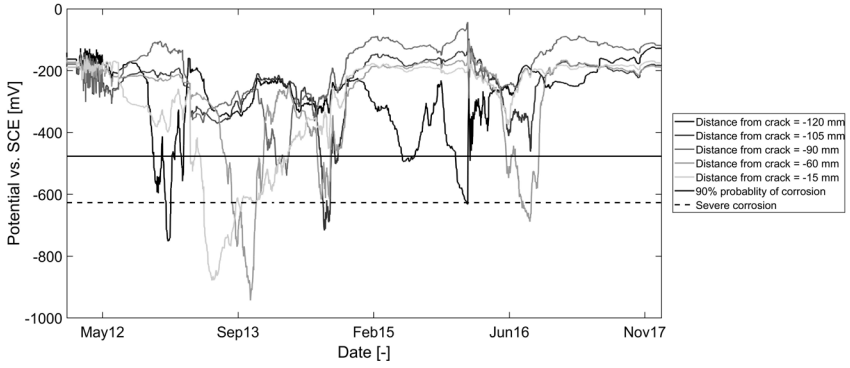

a)

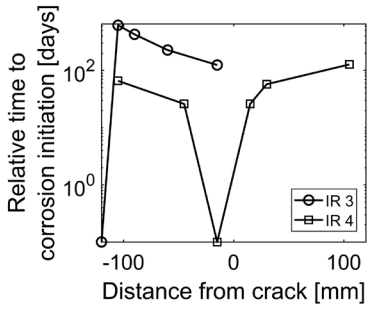

b)

Figure 10: a) Open circuit corrosion potential (OCP) values for IR 3 and indication of limits for 90 % probability and severe corrosion according to [48] and b) calculated relative time to initiation of reinforcement corrosion for selected pins of IR 3 and IR 4, (for location of sensor, see also Figure 1). The indicated time-to-corrosion-initiation along the instrumented rebars is relative to the first recorded time of corrosion initiation.

5 Conclusions

This paper reported results of more than 5 years of continuous *in situ* monitoring of a cracked concrete element exposed to splash and submerged conditions in Rødbyhavn, Denmark. The measurement campaign included monitoring of concrete resistivity, temperature, and open circuit corrosion potential. The use of a custom-built instrumented rebars allowed for crack-distance dependent potential measurements. From the presented depth-dependent resistivity and temperature measurements as well as location- and time-dependent open circuit corrosion potential measurements it may be concluded that:

- For nearly saturated moisture conditions, *i.e.* in the submerged zone, a strong correlation between resistivity and temperature was observed, while this correlation between temperature and resistivity was less pronounced in the splash zone.
- Open circuit corrosion potential measurements indicating active corrosion were first observed after almost two years of exposure for both sensor locations, *i.e.* in the splash and submerged zone. This observation is in strong contrast to many laboratory investigations that have reported corrosion initiation in cracked concrete within days.
- Cycles of OCP indicating depassivation and repassivation were observed with a duration of several years. This discontinuous state of corrosion underlines the importance of continuous monitoring to understand the mechanisms of corrosion initiation and propagation and ultimately the service life of structures.
- The interaction between mass transport, fracture, exposure, and electrochemistry is highly complex and instrumented elements including a variety of sensors for measurement of such features are imperative for model testing to enable accurate and reliable long-term performance predictions of reinforced concrete structures.

Acknowledgements

The authors gratefully acknowledge financial support from Femern Bælt A/S, Sund & Bælt Holding A/S and The Danish Agency for Science, Technology and Innovation, Otto Mønsteds Fond (Grant No. 18-70-1393). The authors' should also like to acknowledge funding from the NPRA R&D program "Ferry-free coastal route E39".

References

[1] U.M. Angst, Challenges and opportunities in corrosion of steel in concrete, Mater. Struct. Constr. 51 (2018) 4. doi:10.1617/s11527-017-1131-6.

[2] O.B. Isgor, A.G. Razaqpur, O. Burkan Isgor, A.G. Razaqpur, Finite element modeling of coupled heat transfer, moisture transport and carbonation processes in concrete structures, Cem. Concr. Compos. 26 (2004) 57–73. doi:10.1016/S0958-9465(02)00125-7.

[3] J. Ožbolt, G. Balabanić, M. Kušter, 3D Numerical modelling of steel corrosion in concrete structures, Corros. Sci. 53 (2011) 4166–4177. doi:10.1016/j.corsci.2011.08.026.

[4] M. Geiker, A. Michel, M.D. Lepech, J. Wu, H. Stang, Multi-scale and multi-physics deterioration modelling for design and assessment of reinforced concrete structures, RILEM Tech. Lett. 2 (2017) 119. doi:10.21809/rilemtechlett.2017.49.

[5] A. Michel, H. Stang, M. Lepech, M.R. Geiker, Multi-Physics and Multi-Scale Deterioration Modelling of Reinforced Concrete, Key Eng. Mater. 665 (2015) 13–16. doi:10.4028/www.scientific.net/KEM.665.13.

[6] A. Michel, Reinforcement Corrosion : Numerical Simulation and Service Life Prediction, Technical University of Denmark (DTU), 2013.

[7] O. Gautefall, Ø. Vennesland, O. Vennesland, Effect of cracks on the corrosion of embedded steel in silica-concrete compared to ordinary concrete, Nord. Concr. Res. 2 (1983) 17–28.

[8] N.S. Berke, M.P. Dallaire, M.C. Hicks, R.J. Hoopes, Corrosion of Steel in Cracked Concrete, CORROSION. 49 (1993) 934–943. doi:10.5006/1.3316020.

[9] T.D. Marcotte, C.M. Hansson, The influence of silica fume on the corrosion resistance of steel in high performance concrete exposed to simulated sea water, J. Mater. Sci. 38 (2003) 4765–4776.

[10] A. Scott, M.G. Alexander, The influence of binder type, cracking and cover on corrosion rates of steel in chloride-contaminated concrete, Mag. Concr. Res. 59 (2007) 495–505. doi:10.1680/macr.2007.59.7.495.

[11] B. Šavija, M. Luković, E. Schlangen, Influence of Cracking on Moisture Uptake in Strain-Hardening Cementitious Composites, J. Nanomechanics Micromechanics. 7 (2017) 04016010. doi:10.1061/(ASCE)NM.2153-5477.0000114.

[12] B. Van Belleghem, R. Montoya, J. Dewanckele, N. Van den Steen, I. De Graeve, J. Deconinck, V. Cnudde, K. Van Tittelboom, N. De Belie, Capillary water absorption in cracked and uncracked mortar – A comparison between experimental study and finite element analysis, Constr. Build. Mater. 110 (2016) 154–162. doi:10.1016/j.conbuildmat.2016.02.027.

[13] A. Michel, B.J. Pease, Moisture ingress in cracked cementitious materials, Cem. Concr. Res. 113 (2018) 154–168. doi:10.1016/j.cemconres.2018.08.009.

[14] D. V. Val, L. Chernin, M.G. Stewart, Experimental and numerical investigation of corrosion-induced cover cracking in reinforced concrete structures, J. Struct. Eng. 135 (2009) 376–385. doi:10.1061/(ASCE)0733-9445(2009)135:4(376).

[15] K. Vu, M.G. Stewart, J. Mullard, Corrosion-induced cracking: Experimental data and predictive models, ACI Struct. J. 102 (2005) 719–726. doi:10.14359/14667.

[16] T.U. Mohammed, H. Hamada, T. Yamaji, Concrete after 30 years of exposure - Part 1: Mineralogy, microstructures,

and interfaces, ACI Mater. J. 101 (2004). https://findit.dtu.dk/en/catalog/2258515551 (accessed June 25, 2019).

[17] L.P. Tang, A. Andersen, Chloride ingress data from five years field exposure in a Swedish marine environment, Rilem Proc. 19 (2000) 105–119.

[18] S.L. Poulsen, H.E. Sørensen, U. Jönsson, Chloride ingress in concrete blocks at the Rødbyhavn marine exposure site - status after 5 years, in: G. Ye, C.R. Rodriguez, H. Zhang, B. Šavija (Eds.), 4th Int. Conf. Serv. Life Des. Infrastructures, RILEM Publications, Delft, 2018: pp. 192–203.

[19] K. Hornbostel, C.K. Larsen, M.R. Geiker, Relationship between concrete resistivity and corrosion rate - A literature review, 2013. doi:10.1016/j.cemconcomp.2013.03.019.

[20] A. Michel, P. V. Nygaard, M.R. Geiker, Experimental investigation on the short-term impact of temperature and moisture on reinforcement corrosion, Corros. Sci. 72 (2013) 26–34. doi:10.1016/j.corsci.2013.02.006.

[21] B. Pease, M. Geiker, H. Stang, J. Weiss, The design of an instrumented rebar for assessment of corrosion in cracked reinforced concrete, Mater. Struct. 44 (2011) 1259–1271. doi:10.1617/s11527-010-9698-1.

[22] H.E. Sørensen, S.L. Poulsen, U. Jönsson, Chloride threshold values form concrete blocks exposed at Rødbyhavn marine field exposure site, in: H.D. Beushausen (Ed.), Performance-Based Approaches Concr. Struct. - 14th Fib Symp. Proc., Cape Town, 2016.

[23] I. Andersen, Salt and temperature conditions in the inner Danish waters, Copenhagen, Danish Meteorological Institute, Technical Report No. 94-4, 1994.

[24] M. Büteführ, C. Fischer, C. Gehlen, K. Menzel, U. Nürnberger, On-site investigations on concrete resistivity – a parameter of durability calculation of reinforced concrete structures, Mater. Corros. 57 (2006) 932–939. doi:10.1002/maco.200604019.

[25] O.E. Gjorv, ELECTRICAL RESISTIVITY OF CONCRETE IN THE OCEANS, Offshore Technol Conf 9th Annu. Proc. 1 (1977). http://findit.dtu.dk/en/catalog?utf8=✓&locale=en&search_field=all_fields&q=Electrical+resistivity+of+concrete (accessed September 14, 2017).

[26] W. Elkey, Electrical resistivity of concrete, 1995. http://findit.dtu.dk/en/catalog?utf8=✓&locale=en&search_field=all_fields&q=Electrical+resistivity+of+concrete (accessed September 14, 2017).

[27] C. Dauberschmidt, J. Harnisch, M. Raupach, Messung des Wassergehaltes von Beton mit Hilfe nachträglich eingebauter Multiring-Elektroden, 2003.

[28] FORCE Technology, FORCE Technology – Catalogue for Products related to Corrosion Monitoring in Concrete, 2017.

[29] A. Michel, A.O.S. Solgaard, B.J. Pease, M.R. Geiker, H. Stang, J.F. Olesen, Experimental investigation of the relation between damage at the concrete-steel interface and initiation of reinforcement corrosion in plain and fibre reinforced concrete, Corros. Sci. 77 (2013) 308–321. doi:10.1016/j.corsci.2013.08.019.

[30] C. Andrade, I.R. Maribona, S. Feliu, J.A. González, S. Feliu, The effect of macrocells between active and passive areas of steel reinforcements, Corros. Sci. 33 (1992) 237–249. doi:10.1016/0010-938X(92)90148-V.

[31] S.P. Holmes, G.D. Wilcox, P.J. Robins, G.K. Glass, A.C. Roberts, Responsive behaviour of galvanic anodes in concrete and the basis for its utilisation, Corros. Sci. 53 (2011) 3450–3454. doi:10.1016/j.corsci.2011.06.026.

[32] M. Alexander, A. Bentur, S. Mindess, Durability of concrete: Design and construction, CRC Press, Boca Raton : CRC Press, [2017] | Series: Modern concrete technology series, 2017. doi:10.1201/9781315118413.

[33] K. Li, Durability design of concrete structures: Phenomena, modelling and practice, John Wiley & Sons, Singapore Pte. Ltd, Singapore, 2016. doi:10.1002/9781118910108.

[34] R.B. Polder, Test methods for on site measurement of resistivity of concrete - a RILEM TC-154 technical recommendation, Constr. Build. Mater. 15 (2001) 125–131. doi:10.1016/S0950-0618(00)00061-1.

[35] M. Castellote, M.C. Alonso, C. Andrade, Standardization, to a reference of 25 degrees celsius of electrical resistivity for mortars and concretes in saturated or isolated conditions, ACI Mater. J. 99 (2002) 119–128. https://findit.dtu.dk/en/catalog/2448190595 (accessed June 21, 2019).

[36] F. Hunkeler, The resistivity of pore water solution - A decisive parameter of rebar corrosion and repair methods, Constr. Build. Mater. 10 (1996) 381–389. doi:10.1016/0950-0618(95)00029-1.

[37] T.M. Chrisp, G. Starrs, W.J. McCarter, E. Rouchotas, J. Blewett, Temperature-conductivity relationships for concrete: An activation energy approach, J. Mater. Sci. Lett. 20 (2001) 1085–1087. doi:10.1023/A:1010926426753.

[38] H.W. Whittington, J. McCarter, M.C. Forde, The conduction of electricity through concrete, Mag. Concr. Res. 33 (2009) 48–60. doi:10.1680/macr.1981.33.114.48.

[39] A. Küter, Management of Reinforcement Corrosion a thermodynamic Approach, PhD thesis, Technical University of Denmark, 2009.

[40] B. Elsener, C. Andrade, J. Gulikers, R. Polder, M. Raupach, Half-cell potential measurements- Potential mapping on reinforced concrete structures, Mater. Struct. 36 (2003) 461–471. doi:10.1617/13718.

[41] P. Schiessl, Zur Frage der zulässigen Rissbreite und der erforderlichen Betondeckung im Stahlbetonbau unter besonderer Berücksichtigung der Karbonatisierung des Betons., Dtsch. Ausschuss Für Stahlbet. 255 (1976). https://findit.dtu.dk/en/catalog/2304985353?single_revert=%2Fen%2Fcatalog%3Fq%3DZur%2BFrage%2Bder%2Bzul%25C3%25A4ssigen%2BRissbreite%2Bund%2Bder%2Berforderlichen%2BBetondeckung%2Bim%2BStahlbetonbau%2Bunter%2Bbesonderer%2BBer%25C3%25BCcksichtigung%2Bder%2B (accessed June 20, 2019).

[42] C. Arya, F.K. Ofori-Darko, Influence of crack frequency on reinforcement corrosion in concrete, Cem. Concr. Res. 26 (1996) 345–353. doi:10.1016/S0008-8846(96)85022-8.

[43] R. Francois, G. Arliguie, Effect of microcracking and cracking on the development of corrosion in reinforced concrete members, Mag. Concr. Res. 51 (1999) 143–150.

[44] A. Michel, M.R.R. Geiker, M. Lepech, H. Stang, Coupled hygrothermal, electrochemical, and mechanical modelling for deterioration prediction in reinforced cementitious materials, in: Proc. 7th Int. Conf. Coupled Probl. Sci. Eng. COUPLED Probl. 2017, 2017: pp. 345–356. https://findit.dtu.dk/en/catalog/2494458928 (accessed September 26, 2019).

[45] C. Edvardsen, Water permeability and autogenous healing of cracks in concrete, Aci Mater. J. 96 (1999) 448–454.

[46] U.M. Angst, M.R. Geiker, A. Michel, C. Gehlen, H. Wong, O.B. Isgor, B. Elsener, C.M. Hansson, R. François, K. Hornbostel, R. Polder, M.C. Alonso, M. Sanchez, M.J. Correia, M. Criado, A. Sagüés, N. Buenfeld, The steel–concrete interface, Mater. Struct. 50 (2017) 143. doi:10.1617/s11527-017-1010-1.

[47] U.M. Angst, M.R. Geiker, M.C. Alonso, R. Polder, O.B. Isgor, B. Elsener, H. Wong, A. Michel, K. Hornbostel, C. Gehlen, R. François, M. Sanchez, M. Criado, H. Sørensen, C. Hansson, R. Pillai, S. Mundra, J. Gulikers, M. Raupach, J. Pacheco, A. Sagüés, The effect of the steel–concrete interface on chloride-induced corrosion initiation in concrete: a critical review by RILEM TC 262-SCI, Mater. Struct. 52 (2019) 88. doi:10.1617/s11527-019-1387-0.

[48] B. Elsener, H. Bohni, Potential mapping and corrosion of steel in concrete, ASTM Spec. Tech. Publ. (1990) 143–156. doi:10.1520/stp25021s.